THESIS

INVESTIGATION OF THE BIOAVAILABILITY OF RADIOCESIUM IN THE FUKUSHIMA EXCLUSION ZONE USING A SEQUENTIAL EXTRACTION TECHNIQUE

Submitted by

Ian McNabb

Department of Environmental and Radiological Health Sciences

In partial fulfillment of the requirements

For the degree of Master of Science

Colorado State University

Fort Collins, Colorado

Spring 2019

Master's Committee:

Advisor: Ralf Sudowe

Thomas Johnson
Thomas Borch

ABSTRACT

INVESTIGATION OF THE BIOAVAILABILITY OF RADIOCESIUM IN THE FUKUSHIMA EXCLUSION ZONE USING A SEQUENTIAL EXTRACTION TECHNIQUE

The nuclear reactor accident at the Fukushima Daiichi power plant in March of 2011, resulted in the release of large quantities of various radionuclides into the environment. The main radionuclide of concern still remaining today is cesium-137 due to its 30-year half-life. Several areas in the vicinity of the power plant are still considered an exclusion zone owing to contamination with radiocesium, and they have not been cleared for human resettlement. While these parts are not suitable for permanent habitation, they are accessible for field work. The purpose of this research was to analyze the movement and bioavailability of radiocesium in the ecosystems contaminated by fallout from the Fukushima Daiichi nuclear reactor accident. This was achieved by analyzing soil cores collected from within the exclusion zone. The core samples were run though a 5-step sequential extraction technique, which exposes the soils stepwise to an increasingly aggressive chemical treatment. Each step targets a specific soil host phase: exchangeable, carbonate bound, Fe/Mn bound, organic, and residual. The results of this extraction yielded the following distribution of Cs-137 activity (percent of total): 0% exchangeable, 1-16% carbonate bound, 0-5% Fe/Mn bound, 1-5% organic, 44-67% residual, and 25-47% non-extracted. These results show that most of the Cs-137 is irreversibly bound to clays in the soil. However there are differences between soil sampling sites in regards to the amount of Cs-137 successfully extracted in the carbonate bound, Fe/Mn bound, and Organic fraction, which

provides evidence that Cs-137 mobility and bioavailability is partly dependent on local soil mineralogy and chemistry.

TABLE OF CONTENTS

ABSTRACT II
CHAPTER 1: INTRODUCTION 1
1.1 Background 1
1.2 Sequential Extraction 2
1.2.1 Exchangeable: 3
1.2.2 Carbonate Bound/Acid Soluble: 3
1.2.3 Fe/Mn oxide Bound: 3
1.2.4 Organic Bound: 4
1.2.5 Residual/Persistently Bound: 4
1.3 Gamma Counting 4
1.3.1 High Purity Germanium Detector 5
1.3.2 Sodium Iodide Detector 7
CHAPTER 2: LITERATURE REVIEW 8
2.1 Cesium Soil Chemistry 8
2.2 Cesium-137 Binding Sites 9
2.2.1 Basal Surface Site 10
2.2.2 Edge Site 10
2.2.3 Frayed Edge Site 11
2.2.4 Interlayer Site 11
2.2.5 Hydrated Interlayer Site 12
2.3 Sequential Extraction Post FDNPP accident 13
2.3.1 Mori et al 2017 13
2.3.2 Tsukada et al 2008 14
2.3.3 Qin 2012 15
CHAPTER 3: MATERIALS & METHODS 17
3.1 Materials 17
3.2 Sampling & Preparation 18
3.3 Sequential Extraction 19
3.4 Counting 21
3.4.1 Sodium Iodide 21
3.3.2 High Purity Germanium 22
CHAPTER 4: RESULTS 24
4.1 Soil Column Activity Profile 24
4.2 Sequential Extraction 25
CHAPTER 5: DISCUSSION 28
5.1 Soil Column Activity Profile 28
5.2 Sequential Extraction 29
REFERENCES 32
APPENDIX I: SEQUENTIAL EXTRACTION PROCEDURE 36
APPENDIX II: RAW DATA 38
Soil Activity Profile 38
Sequential Extraction 39

CHAPTER 1: INTRODUCTION

1.1 Background

On March 11, 2011, a magnitude 9 earthquake hit 130 km off shore directly east of Sendai, Japan. The Great East Japan Earthquake, as it is referred to, gave rise to a massive tsunami that moved towards the east coast of Japan. An hour after the earthquake, the tsunami reached the Fukushima Daichi Nuclear Power Plant (FDNPP) with waves as high as 15 meters. The resulting flooding cut power to the reactors and disabled 12 of the 13 backup generators, thereby making it impossible to provide cooling to three out of the four reactors on site. A nuclear emergency was subsequently declared at 7:00 pm on March 11th. Due to uncontrolled heating of the cores, steam built up inside the reactors. The steam then reacted with the zirconium cladding of the fuel assemblies, creating hydrogen gas in an exothermic reaction. Venting of the hydrogen caused explosions in units one, two, and three, at 25 hour, 87 hours and 68 hours post-earthquake, respectively. These hydrogen explosions blew the roofs of the reactor service halls and resulted in the release of volatile fission products that had been vented from the reactor pressure vessel, most notable iodine-131 with an eight-day half-life, and cesium-137 with a 30-year half-life. The Japanese government estimated a total release of 160 PBq of I-131 and 15 PBq of Cs-137 from the FDNPP. (Hirose 2012)

The surface soil has been removed and stored at temporary storage sites to decontaminate much of the surrounding land. As of January 2018, approximately 16 million m^3 of soil and wastes have been removed. Due to this decontamination effort and many others, the air dose rates have decreased substantially since 2011. Dose rates in decontaminated residential areas have decreased from 1.28 μSv/h to 0.56 μSv/h, which is a 56% decrease. Farmland decreased by

58% and forests by 23%. However, these efforts have been very expensive. Twenty-seven billion USD have been budgeted for the decontamination up to FY2017. In addition, the Japanese government is now faced with the transportation and storage of a large volume of contaminated soils. It poses both an economic issue due to the many man-hours that will need to go into this effort, along with societal problems, due to large storage sites near residential areas. Due to this disaster and the major remediation efforts associated with it, large advancements have been made over the past 7 years in the soil chemistry of cesium. Cesium-137 in particular is the main radionuclide of concern today due to the large amount released into the environment and its persistence due to its 30-year half-life. The advancements in cesium soil chemistry have been aimed in an effort to pioneer new remediation strategies, better understand how cesium moves through the environment and its bioavailability. A better understanding of these characteristics is important because the Fukushima exclusion zone has historically been agricultural land and home to many Japanese citizens. Therefore, by better understanding how cesium interacts with the environment we can better assure safety of the products and people of this region.

1.2 Sequential Extraction

A sequential extraction procedure was utilized to better understand the bioavailability of radiocesium in the Fukushima exclusion zone. Sequential extraction is a technique that successively dissolves soil host phases by a step-wise procedure, exposing the soil to increasingly aggressive chemical treatment. This type of procedure has been utilized for analyzing soils for trace contaminants such as metals and actinides. Sequential extraction explores contaminant mobility in differing environmental conditions, such as changes in pH, redox potential, and addition of organic ligands. (Gleyzes 2002) In each of these conditions the

solubility, which is indicative of mobility and bioavailability, is observed. The most widely used sequential extraction procedure was made by Tessier et al. in 1979. It separated the soil into 5 fractions: Exchangeable, acid soluble, bound to Fe/Mn oxides, oxidizing fraction, and residual. The sequential extraction technique utilized in this research is a version of this technique that was modified by Outola and her coworkers (Outola et al 2009). What follows is an overview of what each fraction in the sequential extraction technique represents and the reagents used to mobilize each of these fractions

1.2.1 Exchangeable:

The exchangeable fraction is comprised of electrostatically bound metal ions in the soil matrix. Cations such as Cs^{+} are attracted to negatively charged complexes in the soil. One of the most predominant negatively charged complexing agents in soil is clay minerals. The reagent used to extract this fraction was a 0.1 M solution of magnesium chloride. Mg^{+2} cations have been shown to replace electrostatically bound cations through a cation exchange reaction.

1.2.2 Carbonate Bound/Acid Soluble:

This fraction is comprised of metals that are co-precipitated with carbonate minerals and specifically sorbed to surface sites of clays and organic matter. In addition, this fraction can extract the remainder of the electrostatically bound species that escaped extraction in the exchangeable fraction (Glyezes 2002). An ammonium acetate/acetic acid buffer solution at a pH of five was utilized to dissolve this fraction.

1.2.3 Fe/Mn oxide Bound:

Iron and manganese oxides have been shown to be the predominate scavengers of metal ions in the soil. Metal ions can coordinate with these oxides exchangeably, moderately fixed

with amorphous oxides, or strongly bound by being occluded within the oxide structures. (Pickering 1986) These oxides can be dissolved by a reducing agent and hydroxylamine was utilized for this purpose in this research.

1.2.4 Organic Bound:

Cesium is a nutrient analogue of potassium, therefore cesium that is not strongly bound to the soil matrix can be taken up by plants and other organisms. A solution of 30% hydrogen peroxide in 0.02M nitric acid at a pH of 2 was used to elute the fraction of cesium available for uptake by plants. Hydrogen peroxide acts as an oxidizing agent to break down organic matter for removal from the soil sample.

1.2.5 Residual/Persistently Bound:

The residual/persistently bound fraction is indicative of metals bound in the crystalline structures of soil minerals. A solution of 4.0 M nitric acid was utilized because it has been shown to break down the crystalline structure of primary and secondary minerals. (Glyezes 2002)

1.3 Gamma Counting

A high purity germanium detector (HPGe) and a sodium iodide detector (NaI) were used to quantify the radiocesium. The HPGe is a semiconductor radiation detector, while the NaI is an inorganic scintillator. Both work by quantifying the energy transferred to orbital electrons of the crystal by incoming gamma radiation. The energy is transferred via three different interactions; photoelectric effect, Compton scattering, or pair production.

The photoelectric effect is the complete transfer of energy from a gamma ray to an orbital electron. The result of this interaction is the disappearance of the incident gamma ray and the orbital electron is liberated and has a kinetic energy equal to the initial energy of the gamma ray

minus its binding energy. This type of reaction creates the photopeak in a gamma spectrum. The photopeak is located at an energy that is equal to the total energy of the incoming gamma radiation.

Compton scattering is the elastic scattering of a photon by an electron. In this type of interaction, the gamma ray only imparts some of its energy to the electron. The amount of energy transferred is dependent on the scattering angle of the gamma radiation. This type of reaction creates the Compton edge in a gamma spectrum because a range of energies can be transferred in this type of interaction, and only some of the initial gamma energy is transferred to the detectors crystal.

Pair production only occurs in high energy gamma radiation (>1.022 MeV). It occurs when a gamma ray spontaneously disappears and creates a positron electron pair. The positron then proceeds to annihilate with a neighboring electron creating two 511 keV gamma rays. The energy from these gamma rays can either be collected by the crystal in subsequent interactions or escape. This type of interaction creates the single and double escape peaks found at 511 keV and 1022 keV.

1.3.1 High Purity Germanium Detector

The HPGe detector is one of the most commonly used gamma spectroscopy instruments. It has many distinguishing characteristics, and pros and cons of its use. The detector is able to quantify the energy of incoming gamma radiation by the following process: First, a voltage is applied across the germanium crystal's volume creating what is known as a depletion region. Within this region no electron hole pairs exist, they have all been driven away by the applied field. Second, gamma radiation emitted from the sample enters the depletion region, interactions and transfers some, or all, of its energy to orbital electrons in the Ge crystal. This transfer of

energy liberates electrons from the valence band, across the band gap, to the conduction band. These electrons then freely travel in the conduction band across the crystal's volume and are collected at the anode. This collection of electrons produces a voltage signal. Third, the external circuit quantifies the amplitude of this voltage signal and provides an output proportional to the energy absorbed within the crystal.

The benefit of using a HPGe detector is its superior energy resolution This is due to the fact that the width of the band gap is only 0.7 eV. Therefore, on average it only takes 2.96 eV to create one electron hole pair in a germanium crystal. This allows for a larger number of charge carriers being created per gamma interaction. This creates a more precise response to a given gamma energy because the inherent statistical fluctuation in the number of charge carriers created is a function of the energy needed to create one electron-hole pair. As shown by the equation below.(W^2_D=inherent statistical fluctuation in the number of charge carriers, F=Fano factor, $\in$=energy necessary to create one electron-hole pair, E=gamma ray energy)

$$W_D^2 = (2.35)^2 F \in E$$

The drawbacks of using a HPGe detector include the necessity of operating the instrument at 77 K. This is to reduce thermally-induced leakage current which is a side effect of the exceedingly small band gap. This is typically achieved by thermally coupling the detector via a copper cooling rod to a dewer of liquid nitrogen. In addition, the HPGe detector has a lower counting efficiency than NaI detectors. This is due to the lower atomic number of Germanium which decreases the probability of a gamma interactions within the crystals volume.

1.3.2 Sodium Iodide Detector

Sodium iodide detectors main contrast with HPGe detectors is that they are scintillator. They quantify the energy of incoming gamma radiation through the following process: First, gamma radiation emitted by the sample enters the sodium iodide crystal and transfers energy to the crystal via the three gamma interactions described above. These interactions provide energy to excite orbital electrons. Second, the electrons deexcite which releases a monoenergetic photon which is picked up by the photomultiplier tube that is adjacent to the crystal. Third, the photons liberate electrons from the photocathode and these electrons are then accelerated across a series of voltage potentials that are designed to emit more electrons at each step, thereby amplifying the electrical signal. Fourth, the electrons are collected and quantified by an external circuit. The amplitude of the voltage signal is proportional to the energy transferred to the NaI crystal by gamma radiation.

The main advantage of using a NaI detector is that they have superior efficiencies. This is due to the fact that the crystal has a higher average Z than Germanium, which increases the probability of gamma ray interaction within the crystal. The main drawback of these detectors is the poor energy resolution. This is due to the fact that the detector converts and amplifies the incoming energy in several steps and each step is venerable to random variation. In addition it requires more energy to excite electrons in the crystal when compared to Ge crystals.

CHAPTER 2: LITERATURE REVIEW

2.1 Cesium Soil Chemistry

In this chapter the current state of knowledge of regarding the chemical behavior of radiocesium in Fukushima soils will be discussed. This includes the types of soils that cesium is most associated within the Fukushima prefecture, a brief discussion of the important physical and chemical properties of these soils, an overview of how cesium ion interacts with various sites on these soil particles, and then finally a summary of recent studies employing sequential extraction techniques used on Fukushima soils post FDNPP accident.

The fact that cesium associates strongly with clay particles in the soil has been known for quite some time. However, the increased research on the soil chemistry of cesium conducted in the aftermath of the FDNPP accident has shown that the majority of cesium in the soils around Fukushima is associated with two clay minerals in particular, illite and biotite. Between these clay minerals it has been shown that cesium-137 preferentially adsorbs to biotite, especially weathered biotite (WB) when present in the soil. (Tanaka 2018). Biotite is also one of the predominant clay minerals found in Fukushima, due to the soil's parent material being weathered granite, which contains biotite. (Okumura 2018)

Both illite and biotite are 2:1 micaceous minerals. This means that they are comprised of two tetrahedral sheets sandwiching an octahedral sheet. In between these sheets is an interlayer space that contains cations, most predominantly potassium. The tetrahedral sheets contain either Al or Si, while the octahedral sheets contain Si, Al, Fe, or Mg. Oxygen and OH groups are then coordinated around these groups in the geometries previously stated. Some important characteristics to consider about these clay minerals when trying to understand their interactions

with cesium include the fact that when these clay minerals weather, isomorphic substitutions occur in both the tetrahedral and octahedral sheets (ex. Al/Si and Mg/Al). This creates a net negative charge for these clays in which the cations present in the interlayer space and the basal surface sites balance. In addition, for these types of clays the interlayer spacing changes during the weathering process. As a result, interlayer cations are lost and predominantly replaced with water. All of these phenomena set the stage for different reaction mechanisms that allow these clay structures to interact with cesium ions. When cesium interacts with these clays they form both inner sphere and outer sphere complexes. It has been shown that a monodentate complex, with mononuclear Cs-O bonds is the most prevalent inner sphere complex formed by cesium with these micaceous clay minerals. This has been observed using Extended X-ray Absorption Fine Structure (EXAFS) spectroscopy. However, Cs-Al and Cs-Si bonds are also likely to be formed, but they have not been successfully identified using this technique (Bostick 2002).

2.2 Cesium-137 Binding Sites

How cesium chemically binds to biotite and illite present in the soil has been summarized very concisely in a recent paper. (Okumura 2018) These binding sites have been studied experimentally and through Monte Carlo modeling techniques. Cesium can interact with these clays at five main binding sites: basal surface sites, edge site, frayed edge sites, interlayer sites, and hydrous interlayer sites. Each of these sites exhibits different binding capacities for cesium along with different binding affinities. And a general depiction of these sites is shown in the figure below.

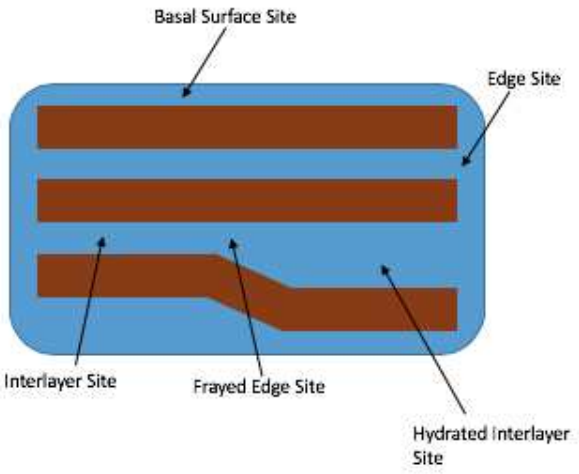

2.2.1 Basal Surface Site

The basal surface site is the binding site with the largest capacity for cesium. However, it has the lowest binding affinity. This site is located on the basal outer surface of the clay minerals. Due to the presence of isomorphic substitutions as stated above, the Cs cations can undergo both an outer-sphere interaction with these sites or inner-sphere interaction. The sites of cesium bonding are strongly associated with the isomorphic substitution sites. These adsorption reactions reach equilibrium rather rapidly and are a very weak, reversible, interaction. This type of bonding is also non-selective for cesium ions.

2.2.2 Edge Site

The edge sites have a much lower capacity for cesium, however, they have a high binding affinity. They also have much slower reaction kinetics than the basal surface sites. In addition the binding appears to be irreversible. These sites are located on the edge of 2:1 clay. The sites are found on anhydrous and non-weathered clay particles. The cesium atom selectively forms an inner-sphere complex at the edge of the interlayer space where the clay structure was broken.

This bond is made with the same periodicity as interlayer cations are bound within the interlayer space of the clay. Cesium preferably binds to hanging sites. Hanging sites are defined as breaks in the clay where the tetrahedral sheet extends past the octahedral sheet. At this location a more 'protected' pocket exists for the cesium atom to occupy (Lammers 2017). The existence of this binding site was shown by Monte Carlo simulation, because up to this point it has not been possible to distinguish this site experimentally from other basal surface sites.

2.2.3 Frayed Edge Site

The frayed edge sites have a much lower capacity for cesium, however, they also have very high binding affinity and the cesium binds to these locations irreversibly. The process of this reaction can be described as follows. Initially, illite is intact with the interlayer of potassium creating a normal 1.0 nm space between the sheets. During weathering, hydrated calcium ions can incorporate into the edge of the interlayer region via ion exchange with potassium. Due to the calcium ions high hydration energy, the ion can remain hydrated in the interlayer space and expand it to a spacing of 1.4 nm. These expanded edge regions are referred to as frayed edge sites (FES). At this point, cesium can now exchange with the calcium via cation exchange. This causes the edges to collapse back down to 1.0 nm. This 'wedge' captures the anhydrous cesium ion at the edge site. This reaction has been shown to be irreversible. This is evident from the fact that if the mineral is re-exposed to calcium, no ion exchange occurs and the calcium does not become re-incorporated at these sites. (Fuller 2015)

2.2.4 Interlayer Site

The interlayer sites have medium capacity for cesium and exhibit a medium affinity. This binding site is indicative of cesium replacing potassium in the interlayer regions of biotite and

illite. This occurs through simple ion exchange. In non-calcium containing weathered biotite and illite, the interlayer cations of these minerals consist predominately of potassium. When cesium is in contact with these clays, the cesium cations undergo cation exchange with the potassium ions and migrate into the mineral interlayer space. The cesium interlayer structure has been shown to be more energetically favorable, so this ion exchange can occur for the entire length of the interlayer channel and lead to complete substitution of all potassium ions. However, the rate of this reaction greatly depends on the local composition of the tetrahedral sheets and how much isomorphic transformations have occurred. (Okumura 2014)

2.2.5 Hydrated Interlayer Site

The hydrated interlayer sites are at the same locations as the interlayer sites discussed above, however, the mechanism of how these sites become occupied by cesium differs slightly. The main difference between the two is that hydrous interlayer sites only occur in weathered illites and biotites. It was shown that as biotite weathers, the Fe^{+2} is oxidized to Fe^{+3}, interlayer cations are lost and replaced by H_2O. (Takashi 2016). Studies found that with increased interlayer hydration of the biotite heavier alkali metal ions were pushed out of the water H-bond network. This net push of cations out of the interlayer space provides the opportunity for cations with low hydration energy to form inner sphere complexes directly with the clay surface. Cesium is the cation most efficiently taken up. The overall effect can be recognized as identical to anhydrous interlayer site bonds, however in this case the H-bond network created by hydration of the interlayer space in these clays is the driving force for the existing cations to be pushed out and vacancies for the cesium cations to be created.

2.3 Sequential Extraction Post FDNPP accident

There have been several studies conducted that utilized sequential extraction techniques to investigate Fukushima soils that contained cesium contamination from the FDNPP accident.

2.3.1 Mori et al 2017

One of such studies was performed by Mori and coworkers (Mori et al 2017). In this study, surface soil samples (down to a depth of 5 cm) were taken from six sites adjacent to Lake Onuma, and one sediment core down to a depth of 50 cm was taken at the center of the lake. Lake Onuma is located 190 km west of FDNPP. All the soils collected had cesium concentration in excess of 500 Bq per kg. After collection of the soil samples, they were air dried at room temperature and sieved to obtain particle sizes <2 mm. All the cesium activity measurements were taken with a HPGe detector. The sequential extraction was performed according to the method described by Tessier (Tessier et al 1979). Fraction 1 (F1) was generated by stirring a mixture of 40 g of the sample and 320 mL of 1 M $MgCl_2$ (pH 7) at ambient temperature for 1 hour. Fraction 2 (F2) was generated by stirring a mixture of the residue of F1 and 320 mL of 1 M CH_3COONa/CH_3COOH (pH 5) at ambient temperature for 5 hours. Fraction 3 (F3) was generated by stirring a mixture of the residue of F2 and 800 mL of 0.04 M NH_2OH-HCl (25% CH_3COOH v/v) at 96 ± 3 °C for 6 hours. Fraction 4 (F4) was generated by stirring a mixture of the residue of F3, 120 mL of 0.02 M HNO_3, and 200 mL of 30% H_2O_2 at 85±2°C for 2 hours, followed by the addition of 120 mL of 30% H_2O_2 with stirring for 3 hours. The sample was then centrifuged to collect the supernatant, to which 200 mL of 3.2 M CH_3COONH_4 solution (20% HNO_3 v/v) was added, diluted with water to a volume of 800 mL, and combined with the previous residue and stirred at ambient temperature for 30 minutes. Fraction 5 (F5) was

generated by drying the residue of F4 at 107 °C in a constant temperature drying oven for over 24 hours.

Each of the five fractions correspond to the following soil host phases: F1 exchangeable, F2 carbonate form, F3 Fe/Mn oxide form, F4 organic form, F5 residual. Each one of the fractions were then filtered and mixed with pure water and measured on the HPGe detector. All samples were counted for 2000 s except for samples containing less than 1 Bq per kg. Those samples were measured for 20,000 s.

The results of their experiment showed that F1 contained 0-1% of the cesium, F2 3-8% F3 12-31%, F4 5-10%, and F5 the majority (75-85%). They concluded from these results that the radiocesium had a low possibility of being released from the soil and therefore was not very bioavailable. In this study they also analyzed the soil using X-ray diffraction (XRD) and observed the peak indicative of Illite being present in the soil. These results could illuminate that the cesium is bound to sites with higher bond strength such as edge sites, or frayed edge sites.

2.3.2 Tsukada et al 2008

Another investigation using sequential extraction was performed on soils in Japan by Tsukada (Tsukada et al 2008). This research predates the FDNPP accident, so the investigation was focused on cesium-137 from global fallout. In this study, 11 soil core samples either 0-5 cm or 0-20 cm depth were collected at agricultural sites in the Aomori prefecture. They were collected in 1991, 1992, 1994, and 2004. The soil samples were dried at 50-60 degrees °C and sieved to 2 mm. The total cesium activity was determined using a HPGe detector. The soil samples were then put through a 2-step sequential extraction technique. In step 1, 80 g of soil sample was extracted with 800 mL CH_3COONH_4 solution (1 M, pH 7) at 20 °C while stirring for 1 hour. For step 2, 40 g of soil sample was suspended in pure water, stirred and heated at 80 C.

Then H_2O_2 (35%), adjusted to pH 2 with HNO_3, was added slowly. In total, approximately 300 ml of H_2O_2 per 40 g soil sample were added over the course of 6 hours. After cooling, 100 mL of 3.2 M CH_3COONH_4 in 20% HNO_3 was added, and the sample was agitated for 30 min.

Each fraction was then measured on a High Purity Germanium detector. The results showed that 12% ± 5% of radiocesium was found in fraction 1, which correlates to exchangeable cesium. In fraction 2, 17% ± 18% of the total radiocesium was found. This fraction corresponds to organically bound cesium. Approximately 70% of the total cesium was found to be in the residual. The results of this study are in agreement with Mori. Most of the cesium was found to be strongly bound to the clays.

2.3.3 Qin 2012

Quinn also performed a sequential extraction on cesium contaminated soil and sediment from the FDNPP accident in Japan (Qin 2012). In addition to conducting sequential extraction experiments, Quin et al. also analyzed the soil using Extended X-ray Absorption Fine Structure (EXAFS) to identify the binding sites of the cesium on the residual soil fraction. EXAFS was used along with XRD to better determine what type of clay minerals were in the samples.

For this study, soil surface samples down to a depth of 5 cm were collected from two location: Kawamata town and Nihonmatsu City, both of which are located in the northern part of the Fukushima prefecture. The samples were collected on May 29th 2011, and from September 17th to December 8th 2011, respectively. The samples were dried at room temperature, sieved through a 2 mm mesh screen and homogenized. The samples were then counted on a High Purity Germanium detector. The sequential extraction protocol fractionated the soil into four soil phases. Briefly, soluble and ligand exchangeable (F1), iron and manganese oxyhydroxide associated (F2), and organic matter and sulphide associated (F3), and the residual fraction (F4).

The fractions were sequentially extracted by acetic acid (0.11 M), hydroxylammonium chloride (0.5 M), and a hydrogen peroxide (8.8 M)/ammonium acetate (1.0 M) solution, respectively and the residual fraction was calculated as the difference between the total Cs-137 activity measured in the soil minus the activity found in the first three fractions.

The result of the XRD analysis showed that clay minerals and micas were present in the soil samples. The total Cs-137 activity in the samples was 48 ± 3.62 Bq/g and 6.28 ± minus 0.2 Bq/g respectively. For soil sample #1, the following percentage of cesium activity was found in each fraction: F1 0.10%, F2 2.81%, F3 3.02%, and F4 94.1%. For sample #2, the result were: F1 0.01%, F2 1.13%, F3 0.6%, and F4 98.3%. These results indicate that most of the cesium-137 was not adsorbed on iron and manganese oxyhydroxides, organic matter, or sulphides. The vast majority remained on the residual phase which supports the hypothesis that most of the cesium is found in interlayer or frayed edge sites. The EXAFS data for this experiment showed that the ratio between outer sphere to inner sphere cesium complexes on the sediment and soil was 0.22 and 0.32 respectively. The difference was attributed to varying organic matter content in the two samples, because organic matter has been shown to play an important role in preventing the coordination of cesium with the siloxane groups to form inner sphere complexes. The difference could also be attributed to the mineralogy of the two samples, because montomorillite is more apt to form outer sphere complexes with cesium than vermiculite or illite. It is important to note that the EXAFS results were obtained after adding stable cesium to the soil samples, because the technique is unable to analyze the trace amounts of radiocesium present in the samples. Under real environmental conditions, with much lower concentrations of cesium, it is hypothesized that the cesium will be preferentially found in inner-sphere complexes because this is much more stable than outer-sphere complexes.

CHAPTER 3: MATERIALS & METHODS

3.1 Materials

- Ammonium acetate, ACS Reagent Grade, Fisher Scientific, Lot#056425
- Acetic acid, glacial, ACS Reagent Grade, J.T Baker, Lot#E1503
- Hydroxylamine; hydrochloride, ACS Reagent Grade, Fisher Scientific, Lot#715834
- Hydrogen peroxide, 30 wt. %, ACS Reagent Grade, Sigma Aldrich, Lot#MKBZ9634V
- Nitric Acid, 67-70% w/w, ACS Grade, VWR Lot#1117070
- Magnesium chloride, ACS Reagent Grade, Sigma Aldrich, Lot#SLBT5102
- Multi-nuclide standard solution, containing Co-57, Co-60, Sr-85, Y-88, Cd-109, Sn-113, Ce-139, Cs-137, Hg-203 & Am-241, Eckert & Ziegler Isotope Products, SN:1815-76
- Gamma verification standard #3, 4-inch Petri dish, flat, (prepared using a multi-nuclide standard solution, containing Co-57, Co-60, Sr-85, Y-88, Cd-109, Sn-113, Ce-139, Cs-137, Hg-203 & Am-241, Eckert & Ziegler Analytics SN: 73061-174)
- Filter, 0.45 μm pore size, 4.75cm diameter
- Drying oven, VWR
- Centrifuge tube, 250 ml
- Nalgene bottles, 500 mL
- Water bath, heated, 75-liter, Thermo Scientific
- Sodium Iodide detector, 3x3 inch, Nucleus
- Coaxial HPGe Detector, P-Type, 35 % relative efficiency, EG&G ORTEC Model GEM-35190-S,

- Centrifuge, Beckman Coulter Allegra 6R

3.2 Sampling & Preparation

Eight 15 cm long soil cores were collected in the Fukushima exclusion zone in June 2013 using an AMS soil core sampler. The location of these sampling sites are shown on figure 1. The cores were then frozen, cut into 2.5 cm segments and stored until November of 2017. The soil segments were then transferred into glass petri dishes and dried at a temperature of 106° C for 12 hours in a VWR drying oven. The soil was then placed into plastic petri dishes and massed.

Figure 1: A Map of the locations were the soil cores were collected in June 2013.

Next, the soil samples were counted on a sodium iodide counter for 24 hours (detailed in the counting section). The most contaminated soil fractions were identified and were then run through the sequential extraction procedure described below.

3.3 Sequential Extraction

Twelve grams of soil were transferred to a 250 mL centrifuge tube. Thirty-five mL of deionized water was added to the tube. The sample was shaken vigorously and allowed to sit overnight. Then 180 mL of a 1M $MgCl_2$ solution was added to the tube. The sample was placed in the water bath shown in figure 2 on the right and kept at a temperature of 25° C for 1 hour. The sample was subsequently centrifuged at 3000 rpm for 25 minutes in the centrifuge shown in figure 2 on the left. The supernatant was poured off the top through a 0.45 μm filter and the filtrate was then transferred to a 500 mL Nalgene bottle. The filtration setup can be seen in figure 3. Twenty-five mL of $MgCl_2$ solution was added to the centrifuge tube containing the sample, mixed, and then centrifuged for 10 minutes at 3000 rpm. The supernatant was again filtered through the same 0.45 μm filter. The filtered rinse was added to the 500 mL Nalgene bottle. Then 25 mL of DI water was added to the sample, mixed, and centrifuged for 10 min at 3000 rpm. The supernatant was again poured off, filtered and added to the 500 mL Nalgene bottle. This procedure was repeated for each step of the sequential extraction technique using the reagents and incubation times outlined in the table 1.

Table 1: Summary of Sequential Extraction Protocol.

Fraction	Reagent	Concentration (M)	T (°C)	Duration (h)
I	$MgCl_2$	0.1	25	1
II	NH_4Ac in 25% (v/v) HAc	1.0	50	2
III	$NH_2OH{\cdot}HCl$ in 25% (v/v) HAc	0.1	70	6
IV	30% H_2O_2 in 0.02 M HNO_3	pH 2	70	3
V	HNO_3	4	90	4

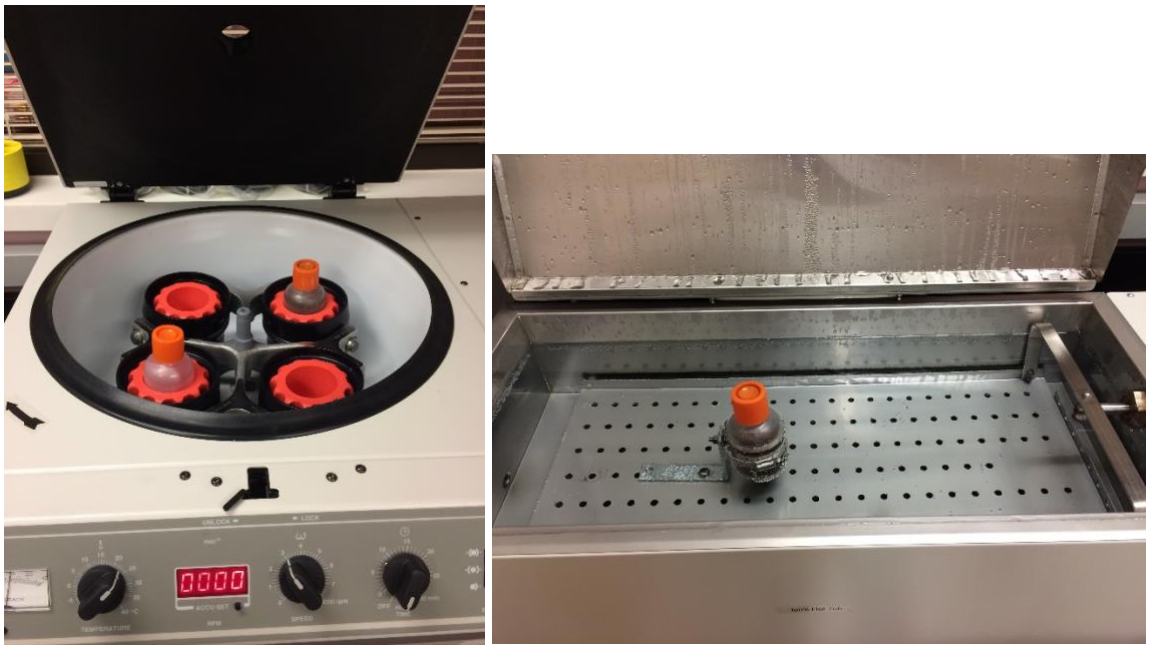

Figure 2: Allegra 6 R centrifuge (left) and Thermo Scientific heated water bath (right) used in the sequential extraction procedure

Figure 3: Filtration apparatus

3.4 Counting

Two instruments, a NaI detector and a HPGe detector, were used during this research along with three different counting geometries to quantify the amount of Cesium-137 present in the soil and each of the sequential extraction fractions.

3.4.1 Sodium Iodide

First, all soil cores in 3 ½ inch petri dishes were counted for 24 hours on a NaI detector (Figure 4). The energy and efficiency calibrations were carried out using the gamma verification standard #3 in a 4-inch flat dish (prepared using Eckert & Ziegler Analytics 73061-174). The standard was counted 24 hours and it had a decay-corrected Cs-137 activity concentration of 0.19 Bq/g (Figure 5).

Figure 4: The sodium iodide detector used to count the Cs-137 activity in the soil.

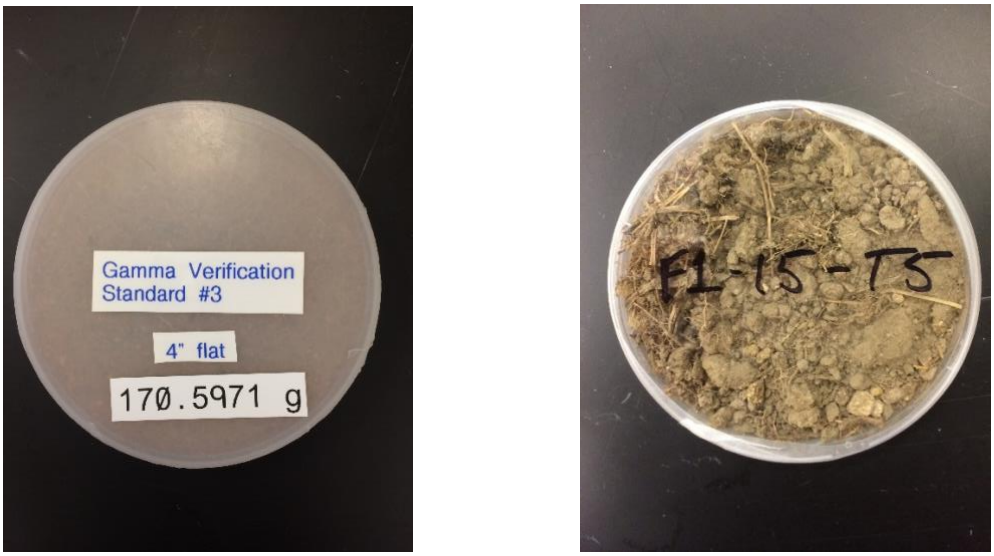

Figure 5: The standard used for efficiency corrections on the NaI detector (left). An example of the soil sample geometry counted on the NaI detector (right).

3.3.2 High Purity Germanium

The soil samples that the sequential extraction procedure was applied to along with the corresponding soil fractions were counted on a HPGe detector, shown in figure 6. The soil was measured before and after the procedure in a 250 mL centrifuge tube. The efficiency for this geometry was calculated by adding 12 g of sand, 30 mL of DI water and 5 mL of the multi nuclide tracer solution purchased from Eckert & Ziegler Isotope Products, that contained 1106.3 Bq of Cs-137, to a 250 mL centrifuge tube. The five soil fractions that were obtained from the procedure were counted in 500ml Nalgene bottles filled with 500 mL of a solution containing the extracted fraction and DI water. The efficiency for this geometry was determined by filling a 500 mL Nalgene bottle with 490 mL of DI water and 10 mL of the multi nuclide tracer solution that contained a total of 2212.6 Bq of Cs-137. The different calibration standards prepared for the measurements can be seen in figure 7.

Figure 6: EG&G ORTEC Co-axial HPGe detector and shielding used to count sequential extraction fractions

Figure 7: The two standards used for efficiency correction on the HPGe detector (left). Examples of the sample geometries counted on the HPGe detector (right).

CHAPTER 4: RESULTS

4.1 Soil Column Activity Profile

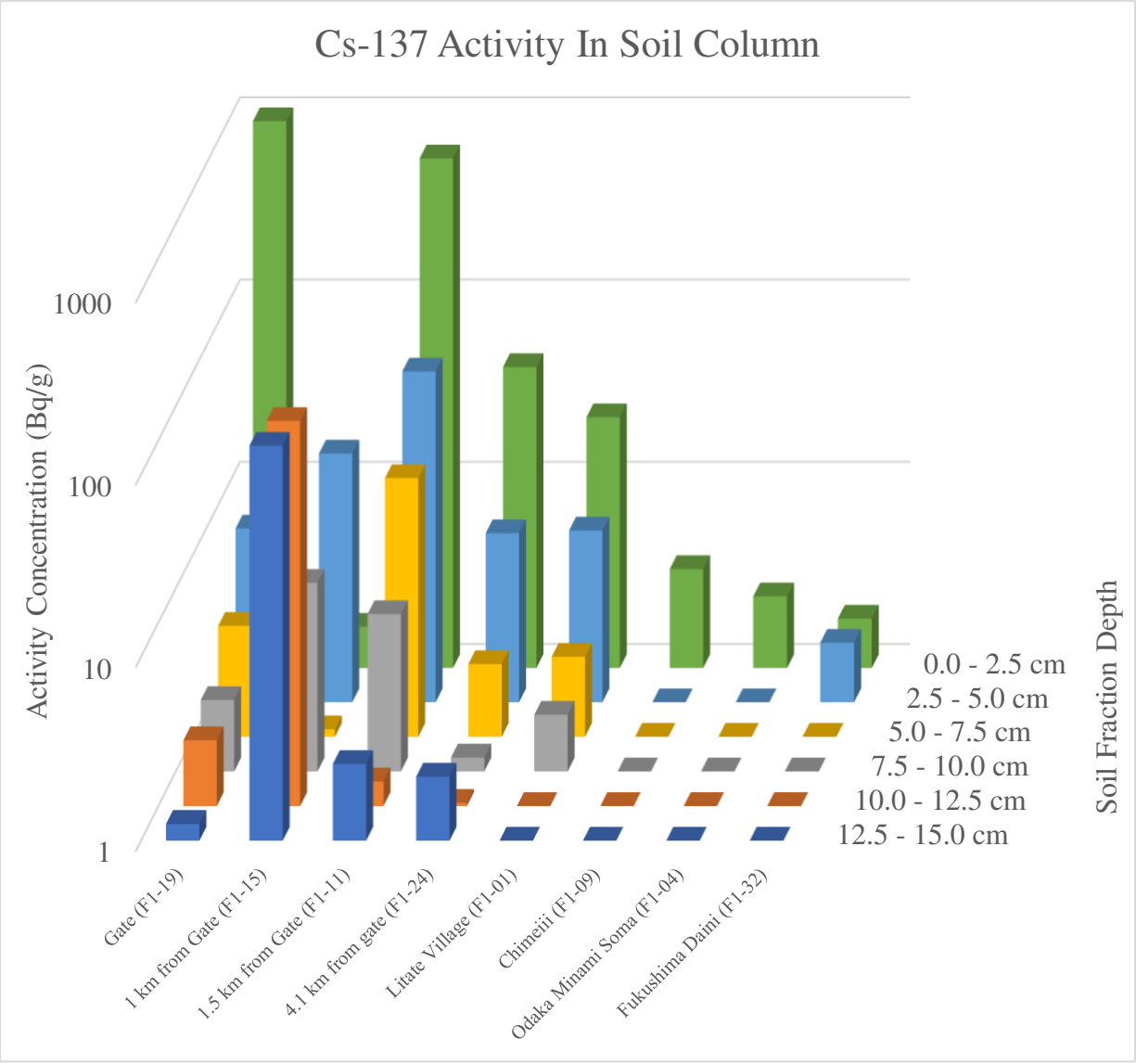

Figure 8: The Cs-137 activity profile of all the soil cores collected from the Fukushima exclusion zone.

The highest Cs-137 activity concentration was seen in the top fraction (0.0-2.5 cm) of soil core F1-19 which was taken at the gate to the reactor site. This sample had an activity

concentration of 1035 Bq/g. The Cs-137 activity in the different cores decreases with increasing distance from the gate. The soil core with the least amount of total activity was soil core F1-04 which had 2 Bq/g of Cs-137 in the top fraction and less than one Bq/g in all deeper fractions. The activity profile for the soil cores follow the same trend with the highest Cs-137 activity at the soil surface with and an approximately exponential decrease in activity down the soil column. The one sample that is the exception to this rule is soil core F1-15. In this soil core the highest activity is in the two deepest fractions (10.0-12.5 cm and 12.5-15.0 cm).

4.2 Sequential Extraction

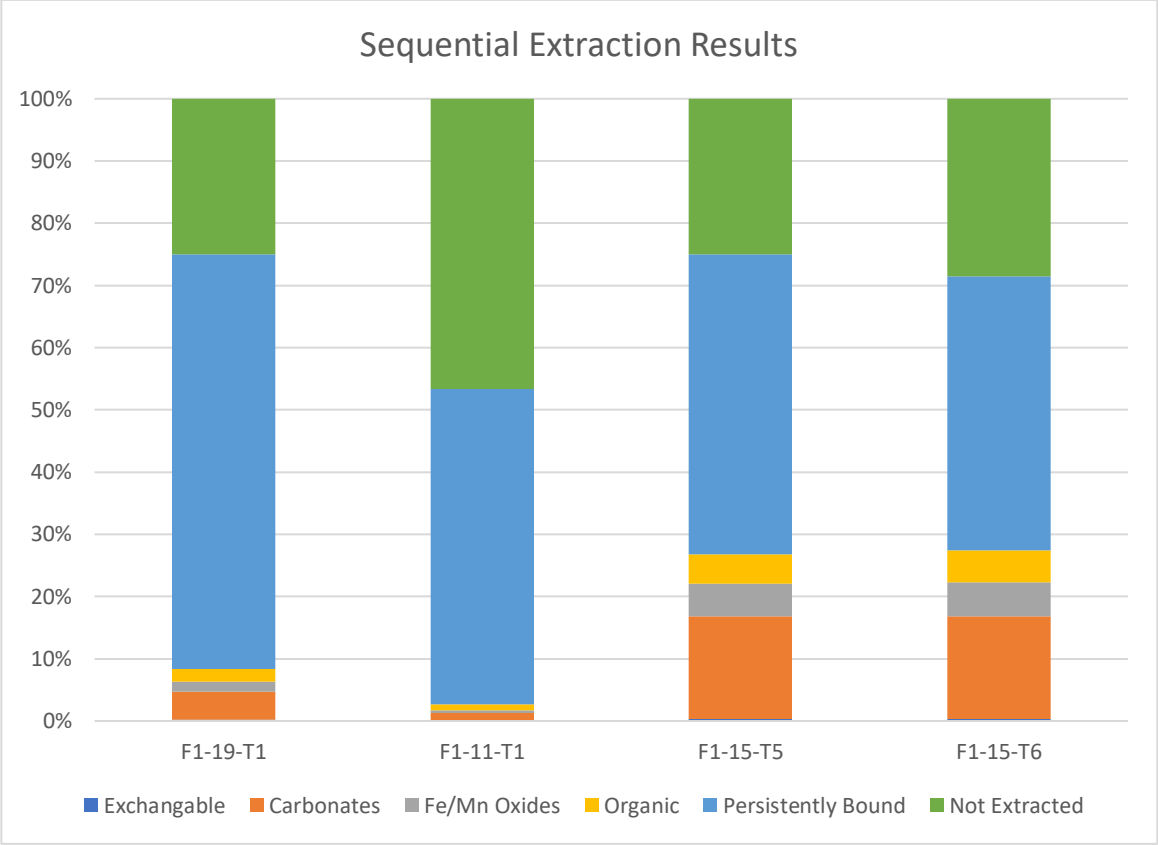

Figure 9: The percent of Cs-137 activity found in each soil fraction in the four soil samples analyzed.

Soil sample F1-19-T1 had most of the Cs-137 activity found in the persistently bound fraction (67%) and in the not extracted fraction (25%). This sample only had 8% of the Cs-137 found in the remaining four fractions. Soil sample F1-11-T1 also had the vast majority of Cs-137 activity in the persistently bound fraction (51%) and not extracted fraction (47%). This sample only had 2% of the Cs-137 activity found in the remaining 4 fractions. Soil samples F1-15-T5 and F1-15-T6 showed very consistent results with one another. Both showed larger percentages of Cs-137 activity in the Carbonate bound phase (16%), Fe/Mn oxide bound phase (5%), and organic bound phase (5%). Even though these soil samples had higher extraction yields in these fractions, still, a large portion of the total activity was found in the persistently bound phase and not extracted phase (73%). The homogeneity of the results from soil sample F1-15-T5 and F1-15-T6 can be attributed to the fact that they are from the same soil core therefore they were collected in the same location as one another and it is highly likely they have nearly identical mineral make up.

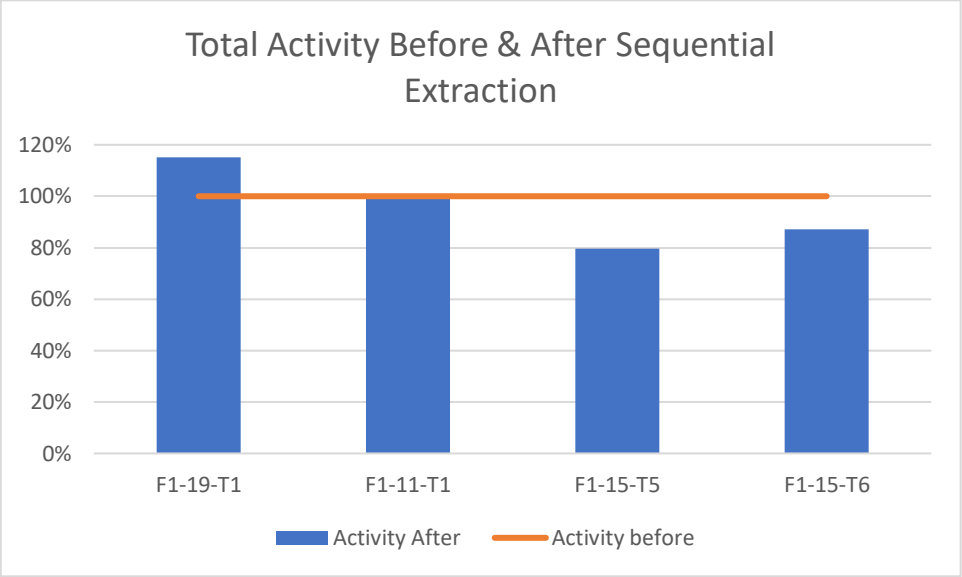

Figure 10: The discrepancy in total activity measured before and after the sequential extraction technique.

The counting results for the four soil samples had some variation. The sum of the F1-19-T1 soil fractions activity was 15% more than the initial activity measurement of the sample before the procedure. While soil sample F1-15-T5 had a 20% loss, and F1-15-T6 had a 13% loss. The possible cause of these discrepancies will be discussed in the following chapter.

CHAPTER 5: DISCUSSION

5.1 Soil Column Activity Profile

The Cs-137 activity profiles of the eight soil cores collected in June of 2013 exhibit three main characteristics that are in agreement with past soil sampling done in the Fukushima exclusion post FDNPP accident (N.Matsuda et al.) These points are; Cs-137 activity approximates an exponential decrease down the soil column, the vast majority of the activity is found in the top 5 cm, and that over time Cs-137 slowly migrates down the soil column.

In the past sampling efforts done in the Fukushima exclusion zone by Matsuda et al., 85 sites were sampled three times between December 2011 and December of 2012. At each site a soil core was taken down to a depth of 8 cm. The cores were split into 5 mm intervals up to the depth of 20 mm, at 10 mm intervals between 20 and 50 mm, and at 30 mm intervals between a depth of 50 and 80 mm. Matsuda showed that the activity profile could be modeled as an exponential decrease of activity down the soil column. This is consistent with the counting results presented above with the exception of soil core F1-15, which will be discussed later.

In addition, Matsuda's results showed that on average 90% of the Cs-137 activity was found in the top 3.01cm (n=82) in December of 2012. While data presented in this work (excluding core F1-15) on average, 86% of the total Cs-137 activity was found in the top 5 cm. This is consistent with Matsuda's data in the sense that most of the activity is still trapped in the top soil layers.

However, the data presented above is not in total agreement with Matsuda's data. This is because the severity of Cs-137 capture in the top few centimeters is less so in this data set compared with Matsuda's. This discrepancy can be due to the fact that Cs-137 slowly migrates

down the soil column and the samples collected for the data set presented above were collected a year after the last samples were collected in Matsuda's data set. However, this migration rate shows significant variability between sample collection sites. For example, sample F1-19 (collected at the gate) had 98% of its Cs-137 remaining in the top 2.5 cm, while soil core F1-15 (collected 1 km from the gate) only had 0.5% of the total Cs-137 activity in the top 2.5 cm. The wide range of Cs-137 activity profile is mostly due to the outlier sample F1-15. This sample's activity profile could possibly be explained by a few different hypotheses. This difference could be due to unnatural mixing of the soil, excessive mixing of the soil by animals or insects, or could possibly be due to differing soil chemistry that allows for the Cs-137 not to be as tightly bound to the soil matrix. The last hypothesis will be discussed further in the sequential extraction discussion section.

5.2 Sequential Extraction

The sequential extraction results first and foremost show that the vast majority of the Cs-137 is very tightly bound to the soil matrix. Between the four samples the percent of radiocesium found in the persistently bound phase and not extracted ranges from 73% (seen in F1-15-T5 and F1-15-T6) up to 98% (seen in F1-11-T1). This finding is consistent with the results by Mori et al. 2017, Qin 2012, and Tsukada et al. 2008 which found 85%, 98.3%, and 70% respectively Cs-137 tightly bound to the soil through their different sequential extraction techniques.

The second important observation of the sequential extraction results is the difference between the Cs-137 activity found in the carbonate bound, Fe/Mn bound, and organic bound phases of the F1-15 cores vs soil cores F1-11 and F1-19. The F1-15 soil cores showed higher extraction in all three of these fractions. Most notably the carbonate bound phase where F1-15 cores had 16% of the Cs-137 activity in this fraction compared to 4% and 1% in soil cores F1-19

and F1-11 respectively. These results provide evidence that the Cs-137 is less tightly bound to the soil in core F1-15 than the Cs-137 found in the other soil samples. This can be further supported by soil core F1-15's activity profile. It was shown that in this soil core more Cs-137 activity was found deeper in the soil than the surface layers. F1-15-T5 was harvested 10.0 cm – 12.5 cm below the surface and F1-15-T6 was harvested 12.5 cm -15.0 cm below the surface. This shows that the Cs-137 was able to percolate down the soil column much more readily than the other cores. The fact that the sequential extraction results show that the Cs-137 is less tightly bound to the soil and that the soil core activity profile show these attributes it gives evidence for two conclusions. One, this procedure can provide meaningful results to predict the mobility of Cs-137 in soil. Two, the fact that the local soil minerology, and chemistry has an effect on Cs-137 mobility and bioavailability.

The results of the sequential extraction technique also provides evidence to what binding sites (detailed in the literature review section) the Cs-137 molecules are predominantly located. Since most of the activity was found in the persistently bound phase or not extracted from the soil at all most of the radiocesium is most likely bound to clay minerals present in the soils. Although, the specific clay mineral species were not identified in the soil samples in this research, past sampling and identification via EXAFS by (Qin 2012) showed that illite and biotite is abundant in Fukushima prefecture soils. Therefore, it is likely that the radiocesium is bound in the edge sites and interlayer sites in this mineral. This is because these two binding sites have been shown to have the highest binding affinities and a higher abundance of inner sphere complexes (Okumura et al. 2018). The radiocesium in these sites was partly extracted by the 4.0 M nitric acid because nitric acid can start to break down the crystalline structure of primary and secondary minerals (Faye 2014) and thereby release the cesium bound in the interlayer and edge

sites. However, the 4.0 M nitric acid is unable to completely break down the crystalline structure as seen by the result that large portions of the total activity are unable to be extracted with this technique.

The second point of discussion of the result obtained from the sequential extraction technique is the discrepancy of total activity before and after the procedure. The loss seen in F1-15-T5 and F1-15-T6 could be attributed to insufficient washing of filters between fractions. Some soil particles could be left on the filter and thrown out which would create some loss. On the other end of the spectrum soil sample F1-19-T1 showed a gain of activity in the samples after the sequential extraction procedure. No activity could have possibly been gained by this procedure, so this discrepancy is most likely to counting efficiency errors. The counting standard approximated the same geometries however there are differences in the soil types between the samples and there could be greater attenuation in one compared with the others.

REFERENCES

1. Bostick, Benjamin C., et al. "Cesium adsorption on clay minerals: An EXAFS spectroscopic investigation." *Environmental Science & Technology* 36.12 (2002): 2670-2676.
2. Brouwer, E., Baeyens, B., Maes, A., & Cremers, A. (1983). Cesium and rubidium ion equilibriums in illite clay. *The Journal of Physical Chemistry*, *87*(7), 1213-1219.
3. Byrnes, I., Johnson, Thomas E., Borch, Thomas, & Brandl, Alexander. (2017). *Radiocesium Dynamics in Irrigation Ponds in Okuma, Japan,* ProQuest Dissertations and Theses.
4. *Environmental Remediation in Japan* (Rep.). (2018). Ministry of the Environment.
5. Faye, S., Sudowe, Ralf, Buck, Brenda, Hodge, Vernon, & Inn, Kenneth. (2014). *Simultaneous Determination of Multiple Actinide Elements in a Variety of Soils Utilizing a Standardized Sequential Extraction Protocol,* ProQuest Dissertations and Theses.
6. Fuller, A. J., Shaw, S., Ward, M. B., Haigh, S. J., Mosselmans, J. F. W., Peacock, C. L., ... & Burke, I. T. (2015). Caesium incorporation and retention in illite interlayers. *Applied Clay Science*, *108*, 128-134.
7. Gleyzes, Christine, Sylvaine Tellier, and Michel Astruc. "Fractionation studies of trace elements in contaminated soils and sediments: a review of sequential extraction procedures." *TrAC Trends in Analytical Chemistry* 21.6-7 (2002): 451-467.
8. Hirose, Katsumi. "2011 Fukushima Dai-ichi nuclear power plant accident: summary of regional radioactive deposition monitoring results." *Journal of environmental radioactivity* 111 (2012): 13-17.

9. Ikeda, T. (2016). First-principles-based simulation of interlayer water and alkali metal ions in weathered biotite. *The Journal of Chemical Physics*, *145*(12), 124703.
10. Lammers, L. N., Bourg, I. C., Okumura, M., Kolluri, K., Sposito, G., & Machida, M. (2017). Molecular dynamics simulations of cesium adsorption on illite nanoparticles. *Journal of colloid and interface science*, *490*, 608-620.
11. Matsuda, N., Mikami, S., Shimoura, S., Takahashi, J., Nakano, M., Shimada, K., ... & Saito, K. (2015). Depth profiles of radioactive cesium in soil using a scraper plate over a wide area surrounding the Fukushima Dai-ichi Nuclear Power Plant, Japan. *Journal of environmental radioactivity*, *139*, 427-434.
12. Mori, M., Tsunoda, K. I., Aizawa, S., Saito, Y., Koike, Y., Gonda, T., ... & Tanaka, H. (2017). Fractionation of radiocesium in soil, sediments, and aquatic organisms in Lake Onuma of Mt. Akagi, Gunma Prefecture using sequential extraction. *Science of the Total Environment*, *575*, 1247-1254.
13. Okumura, Kerisit, Bourg, Lammers, Ikeda, Sassi, . . . Machida. (2018). Radiocesium interaction with clay minerals: Theory and simulation advances Post–Fukushima. *Journal of Environmental Radioactivity, 189*, 135-145.
14. Okumura, T., Tamura, K., Fujii, E., Yamada, H., & Kogure, T. (2013). Direct observation of cesium at the interlayer region in phlogopite mica. *Microscopy*, *63*(1), 65-72.
15. Outola, I., Inn, K., Ford, R., Markham, S., & Outola, P. (2009). Optimizing standard sequential extraction protocol with lake and ocean sediments. *Journal of radioanalytical and nuclear chemistry*, *282*(2), 321-327.
16. Pickering, W. F. "Metal ion speciation—soils and sediments (a review)." *Ore Geology Reviews* 1.1 (1986): 83-146.

17. Qin, H., Yokoyama, Y., Fan, Q., Iwatani, H., Tanaka, K., Sakaguchi, A., ... & Takahashi, Y. (2012). Investigation of cesium adsorption on soil and sediment samples from Fukushima Prefecture by sequential extraction and EXAFS technique. *Geochemical Journal*, *46*(4), 297-302.
18. Rauret, G., Lopez-Sanchez, J. F., Sahuquillo, A., Rubio, R., Davidson, C., Ure, A., & Quevauviller, P. (1999). Improvement of the BCR three step sequential extraction procedure prior to the certification of new sediment and soil reference materials. *Journal of Environmental Monitoring*, *1*(1), 57-61.
19. Rosenberg, B., Brandl, Alexander, Borch, Thomas, Henry, Charles, Pinder, John, & Steinhauser, Georg. (2016). *Analytical Methods to Enhance Detection of Anthropogenic Radionuclides in Environmental Matrices,* ProQuest Dissertations and Theses.
20. Tack, Filip M., and Marc G. Verloo. "Impact of single reagent extraction using NH4OAc-EDTA on the solid phase distribution of metals in a contaminated dredged sediment." *Science of the Total Environment* 178.1-3 (1996): 29-36.
21. Takahashi, Y., Fan, Q., Suga, H., Tanaka, K., Sakaguchi, A., Takeichi, Y., ... & Kanivets, V. V. (2017). Comparison of solid-water partitions of radiocesium in river waters in Fukushima and Chernobyl areas. *Scientific reports*, *7*(1), 12407.
22. Tanaka, K., Watanabe, N., Yamasaki, S., Sakaguchi, A., Fan, Q., & Takahashi, Y. (2018). Mineralogical control of the size distribution of stable Cs and radiocesium in riverbed sediments. *Geochemical Journal*, *52*(2), 173-185.
23. Tessier, A., Campbell, P. G., & Bisson, M. (1979). Sequential extraction procedure for the speciation of particulate trace metals. *Analytical chemistry*, *51*(7), 844-851.

24. Tsukada, H., Takeda, A., Hisamatsu, S. I., & Inaba, J. (2008). Concentration and specific activity of fallout 137Cs in extracted and particle-size fractions of cultivated soils. *Journal of environmental radioactivity*, *99*(6), 875-881.

APPENDIX I: SEQUENTIAL EXTRACTION PROCEDURE

Fraction	Reagent	Concentration (M)	T (°C)	Duration (h)
I	$MgCl_2$	0.1	25	1
II	NH_4Ac in 25% (v/v) HAc	1.0	50	2
III	$NH_2OH{\cdot}HCl$ in 25% (v/v) HAc	0.1	70	6
IV	30% H_2O_2 in 0.02 M HNO_3	pH 2	70	3
V	HNO_3	4	90	4

1. Dry sediment overnight at 60° C in a thermostatically controlled oven.
2. Weigh 12g of soil into 250ml centrifuge tube.
3. Add 35 mL deionized water to expand clay minerals, mix vigorously, allow to sit overnight.
4. Add 180 mL of the extracting reagent (outline in the table above) to the centrifuge bottle containing sediment.
5. Cap bottle and place in water bath set to the temperature and reaction time shown in the table above.
6. Remove centrifuge bottle from water bath.
7. Centrifuge bottle at 3000 rpm for 25 minutes.
8. Decant and filter supernatant through 0.45 μm filter.
9. Rinse residual sediment with 25 mL of the extracting reagent.
10. Centrifuge at 3000 rpm for 10 minutes.
11. Decant and filter supernatant through 0.45 μm filter.
12. Rinse the residual sediment with 25 mL DI water.
13. Centrifuge at 3000 rpm for 10 minutes.
14. Decant and filter supernatant through 0.45 μm filter.

15. Transfer the filtrate into a 500 mL Nalgene bottle.
16. Place the filter in the centrifuge bottle with the sediment to be rinsed before the next extraction.
17. Acidify the filtrate to pH 1 with 4.0M HNO_3.
18. Add additional DI water to Nalgene bottle until the net weight of the sample is 500g.
19. Save sample for gamma spectroscopy.
20. Repeat steps 1-19 for fractions II, III, and V.
21. For fraction IV, add 70 mL of 0.02 HNO_3 to the centrifuge tube containing the sediment.
22. Place the bottle in a 70° C water bath.
23. Add 110 mL of H_2O_2 drop wise, with occasional agitation, until reaction is complete. This should take approximately 3 hours. Monitor pH and keep close to 2.
24. Repeat steps 7-19.

APPENDIX II: RAW DATA

Soil Activity Profile

	0.0-2.5 cm	**2.5-5.0 cm**	**5.0-7.5 cm**	**7.5-10.0 cm**	**10.0-12.5 cm**	**12.5-15.0 cm**
Gate (F1-19)	1044.68	9.05	4.08	2.46	2.29	1.24
1 km from Gate (F1-15)	1.70	23.35	1.11	10.83	129.05	145.26
1.5 km from Gate (F1-11)	631.43	65.86	26.40	7.30	1.37	2.63
4.1 km from gate (F1-24)	45.24	8.54	2.52	1.20	1.05	2.24
Litate Village (F1-01)	23.98	8.83	2.76	2.05	0.85	0.68
Chimeiii (F1-09)	3.53	0.56	0.22	0.23	0.22	0.42
Odaka Minami Soma (F1-04)	2.49	0.24	0.21	0.19	0.21	0.17
Fukushima Daini (F1-32)	1.88	2.14	0.28	0.25	0.25	0.26

*Units of Bq/g decay corrected to March 2011

Sequential Extraction

	F1-11-T1	F1-19-T1	F1-15-T6	F1-15-T5
Before	8970	17452	3206	3482
Fraction1	7	43	11	10
Fraction2	108	901	461	456
Fraction3	37	321	151	147
Fraction4	86	412	145	130
Fraction5	4577	13390	1230	1335
After	4205	5014	797	694

*Units in Bq